Argon diffusion in plagioclase and implications for thermochronometry: A case study from the Bushveld Complex, South Africa

William S. Cassata [a,b,*], Paul R. Renne [a,b], David L. Shuster [b]

[a] *Department of Earth and Planetary Sciences, University of California – Berkeley, 307 McCone Hall #4767, Berkeley, CA 94720-4767, USA*
[b] *Berkeley Geochronology Center, 2455 Ridge Road, Berkeley, CA 94709, USA*

Abstract

Plagioclase is not only the most abundant mineral in the Earth's crust, but is present in almost all terrestrial tectonic settings and is widespread in most extraterrestrial material. Applying the K–Ar system to this common mineral would provide a powerful tool for quantifying thermal histories in a wide variety of settings. Nonetheless, plagioclase has rarely been used for thermochronometry, largely due to difficulties in simultaneously acquiring precise geochronologic data and quantifying argon diffusion kinetics from a mineral with low-K concentration. Here we describe an analytical technique that generates high-precision $^{40}Ar/^{39}Ar$ data and quantifies Ar diffusion kinetics of low-K minerals. We present results of five diffusion experiments conducted on single crystals of plagioclase from the Bushveld Complex, South Africa. The observed diffusion kinetics yield internally consistent thermochronological constraints, indicating that plagioclase is a reliable thermochronometer. Individual grains have activation energies of 155–178 kJ/mol and $\ln(D_0/a^2)$ varies between 3.5 and 6.5. These diffusion parameters correspond to closure temperatures of 225–300 °C, for a 10 °C/Ma cooling rate. Age spectra generally conform to single-domain diffusive loss profiles, suggesting that grain-scale diffusion dominates argon transport in this fairly simple plagioclase. Conjointly examining several single-grain analyses enables us to distinguish episodic reheating from slow cooling and indicates that the Bushveld Complex cooled rapidly and monotonically from magmatic temperature to <300 °C over 3 Ma, followed by protracted cooling to ambient crustal temperatures of 150–200 °C over ~600 Ma.
© 2009 Elsevier Ltd. All rights reserved.

1. INTRODUCTION

The mechanisms and kinetics of argon (Ar) diffusion in the crust and mantle are critical to many topics in the Earth and planetary sciences. Despite being the most abundant mineral in the crust and one commonly used for $^{40}Ar/^{39}Ar$ geochronology, plagioclase has not routinely been used for thermochronometry. Most $^{40}Ar/^{39}Ar$ thermochronometry has focused on potassium (K) rich minerals such as micas, amphiboles, and alkali feldspars owing to the relative ease with which Ar measurements can be made (McDougall and Harrison, 1999). However, as plagioclase is often the only K-bearing mineral in meteorites, lunar rocks, layered mafic intrusions, mafic dike swarms, flood basalts, ophiolites, and major basaltic sill complexes, its use for thermochronometry holds tremendous potential. Attempts to constrain the thermal histories of these rocks have generally relied upon theoretical modeling, without direct thermochronometric constraints (e.g., Hess and Parmentier, 1995; Cawthorn and Walraven, 1998). $^{40}Ar/^{39}Ar$ thermochronometry of plagioclase offers direct, observational constraints of thermal histories after crystallization. Ar diffusion kinetics and $^{40}Ar/^{39}Ar$ ages of plagioclase would

* Corresponding author. Address: Department of Earth and Planetary Sciences, University of California – Berkeley, 307 McCone Hall #4767, Berkeley, CA 94720-4767, USA.

   E-mail addresses: cassata@berkeley.edu (W.S. Cassata), prenne@bgc.org (P.R. Renne), dshuster@bgc.org, tbecker@bgc.org (D.L. Shuster).

also be useful for constraining thermal histories of diverse geological settings including mountain belts, metamorphic terrains, and sedimentary basins.

Few published data exist to quantify the diffusion kinetics of argon in plagioclase, and none are sufficiently precise for high-resolution thermochronometry. Fechtig et al. (1960) first reported diffusion parameters for plagioclase, based on analyses of reactor-produced ^{37}Ar in anorthite. Berger and York (1981) reported results from six plagioclase samples using the formulae of Fechtig and Kalbitzer (1966) applied to data acquired in routine step-heating ^{40}Ar/^{39}Ar experiments configured for age spectrum analysis. Subsequent studies by Harrison and McDougall (1981), Renne et al. (1990), Onstott et al. (1989), Renne et al. (1996), Boven et al. (2001), and Garrick-Bethell et al. (2009) also reported diffusion parameters from routine step-heating ^{40}Ar/^{39}Ar experiments on plagioclase. These studies used various combinations of ^{40}Ar*, ^{39}Ar, and ^{37}Ar as the diffusant and a variety of temperature controlling and measurement techniques. The results-unmodified from values cited in the original sources- are summarized in Fig. 1.

In general, Arrhenius plots calculated from these experiments do not reveal simple linear arrays. The inferred activation energies (E_a) and frequency factors ($\ln(D_0/a^2)$) are commonly constrained from the lowest temperature data that yield a linear array in $\ln(D_0/a^2)$ vs. T^{-1}; Fig. 1 shows the range in published E_a and D_0/a^2 values. In most cases, the selection of regressed data appears somewhat subjective, and most are based on <10 steps. Many of the studies do not report uncertainties in E_a and $\ln(D_0/a^2)$. In some instances, temperature and isotope signal/abundance data required to redraft Arrhenius plots are not published. Some studies (e.g., Harrison and McDougall, 1981) used plane slab (infinite sheet) diffusion geometry, but most used spherical geometry to compute $D(T)$ values. Nonetheless, the range of diffusion parameters shown in Fig. 1 far exceeds what is expected from different choices of diffusion

geometry or data selection, and certainly exceeds the range expected from the typical reported uncertainties. While it is likely that the range of D_0/a^2 values is partly due to size differences between the analyzed samples, the parameter "a" would have to vary by five orders of magnitude to fully explain the data. The activation energies show a broad correlation with $\ln(D_0/a^2)$, which could be a consequence of the Meyer–Neldel compensation rule (Meyer and Neldel, 1937) or could indicate correlated errors. Whatever the source of variation, the published results suggest that plagioclase has a wide range in Ar closure temperature, from <0 to 500 °C.
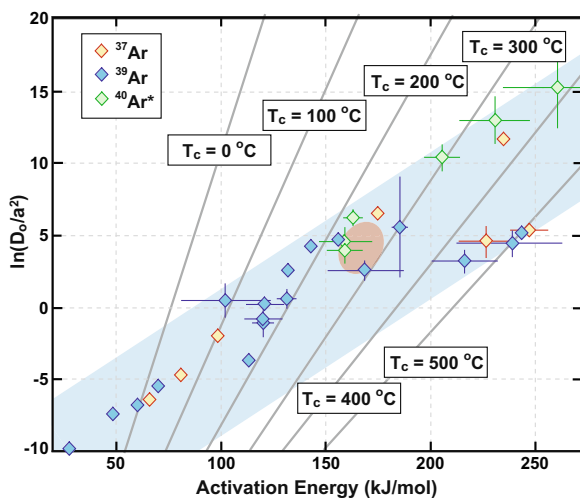
To determine whether Ar diffusion kinetics can be reproduced for a given sample, and to assess the potential utility of plagioclase for Ar thermochronometry, we conducted a series of diffusion experiments (coupled with ^{40}Ar/^{39}Ar analyses) on plagioclase from a gabbro in the Bushveld Complex of South Africa. Our inferred diffusion parameters and ^{40}Ar/^{39}Ar ages yield internally consistent information, suggesting that the K–Ar system in plagioclase records thermochronological information. We use the set of observations to constrain the thermal history of the Bushveld Complex below ∼350 °C at this locality. We also describe our analytical apparatus designed to collect high-precision ^{40}Ar/^{39}Ar data and Ar diffusion kinetics from single grains of low-K minerals, using extraction temperatures between 350 and 1200 °C.

2. GEOLOGIC SETTING AND SAMPLE LOCALITY

The Bushveld Complex of eastern South Africa is the largest layered mafic intrusion in world, comprising over 500,000 km^3 of primarily mafic igneous rocks with minor amounts of silicic rocks near the roof. The mafic portion of the intrusion has an average thickness of 8 km and can be divided into five zones: the marginal, lower, critical, main and upper zones, collectively composing the Rustenburg Layered Suite (RLS) (Fig. 2). The intrusion is thought by some to have resulted from a mantle-derived magma plume (Campbell et al., 1989) and may be the sub-volcanic root of an eroded continental flood basalt province (e.g., Cawthorn and Walraven, 1998). The Bushveld Complex was built by a series of intrusive pulses (Eales and Reynolds, 1986) whose tempo is poorly constrained but has been inferred to involve 12 magma pulses emplaced in <100 ka (e.g., Cawthorn and Walraven, 1998). Rapid emplacement and cooling, at least of the western limb of the Complex, is supported by limited ^{40}Ar/^{39}Ar (biotite) and U/Pb (zircon and rutile) studies (Nomade et al., 2004; Scoates and Friedman, 2008) of the platiniferous UG-2 and Merensky Reef horizons, respectively. Based on an inferred 1% bias between commonly-used calibrations of the U/Pb and ^{40}Ar/^{39}Ar systems, Nomade et al. (2004) suggested that a cooling rate of ca. 1000 °C/Ma between 700 and <500 °C was implied by comparison of their data with those of Buick et al. (2001).

Fig. 1. Kinetic parameters for diffusion of ^{40}Ar*, ^{39}Ar, and ^{37}Ar in plagioclase from existing data (see text for sources). Lines correspond to closure temperatures between 0 and 500 °C calculated for 10 °C/Ma (Dodson, 1973). The red oval spans the range of diffusion parameters presented in this paper.

3. SAMPLE BV-8

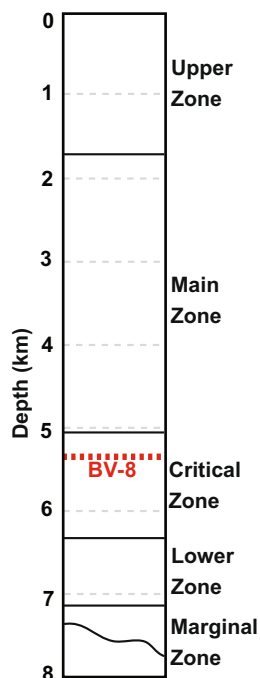Sample BV-8 is a gabbro near the MG-1 chromite layer in the critical zone of the Rustenburg Layered Suite. The

Fig. 2. Schematic stratigraphic column of the western limb of the Bushveld Complex (unit thicknesses from Cawthorn and Walraven, 1998). The dashed red line denotes the location of sample BV-8. (For interpretation of the references to color in this figure legend, the reader is referred to the web version of this paper.)

sample was collected at the Hernic Ferrochrome Mine near the town of Brits (western limb), at 25° 39.537′S latitude, 27° 50.774′E longitude. The gabbro comprises clinopyroxene, orthopyroxene, plagioclase, biotite, and trace quantities of K-feldspar, quartz, and chromite. Plagioclase is an intercumulus phase, with poikilitic crystals that are compositionally bimodal (An_{70} and An_{40} populations). Electron microprobe analyses (methods detailed in Jourdan and Renne, 2007) indicate K_2O concentration is typically 0.2 wt.%. Individual plagioclase grains are 0.5–1.5 mm in diameter and are compositionally homogenous at the μm scale (Fig. 3). Although nanometer-scale anti-perthite lamellae may exist, reactor-induced ^{37}Ar and ^{39}Ar recoil would likely obscure any compositional variations of this lengthscale. Most grains are considerably zoned, with higher K and lower Ca concentrations toward the marginal ~3% of the grain (Fig. 3). Although marginally zoned grains seemingly violate the homogeneity criterion for diffusion calculations, the effect is easily identified and accurate diffusion parameters are obtainable from these samples, as discussed later.

Three incremental-heating analyses of single crystals of BV-8 plagioclase revealed relatively simple age spectra characteristic of single-domain diffusive loss profiles, with different apparent plateau ages ranging from 2019 ± 9 to 2040 ± 9 Ma (Electronic Annex Fig. 1). The ages of the initially extracted, low-temperature steps range from ~1.3 to 1.6 Ga, with fairly large uncertainties. The observed age spectra may be explained by slow cooling and protracted residence at elevated crustal temperature or episodic loss of ^{40}Ar due to reheating by younger intrusions such as

the nearby ~1.4 Ga Pilanesburg Complex. Because a single crystal of BV-8 biotite yielded a 100% concordant age spectrum (Electronic Annex Fig. 1) indistinguishable from U/Pb ages (see Section 6), the plagioclase age spectra must have resulted from incomplete ^{40}Ar retention at temperatures significantly below the biotite closure temperature ($T_c = 300–450 °C$, McDougall and Harrison, 1999). The range in apparent plateaus ages indicates that the ^{40}Ar retentivity of these plagioclase grains is variable. Our data reveal grain-specific diffusion kinetics and confirm that the age differences are related to inherent diffusion properties of each crystal. We use the observed kinetics to differentiate between late-stage episodic loss and slow cooling to constrain the thermal history of the Bushveld Complex.

4. ANALYTICAL METHODS

4.1. Experimental design

To test for correlations between the observed age differences and Ar retentivity, it was necessary to simultaneously collect both $^{40}Ar/^{39}Ar$ data and diffusion parameters from single crystals of plagioclase. To extract Ar at the lowest temperatures at which measurable argon ion beams can be generated on reasonable laboratory timescales required the lowest possible procedural blanks. To achieve this, we developed a technique whereby single crystals were wrapped in small, previously degassed platinum–iridium (Pl–Ir) envelopes and heated with a diode laser. Temperature was measured with an optical pyrometer and controlled between 350 and 1200 °C with ±5 °C accuracy with a high-frequency feedback loop.

Previous diffusion studies on feldspars have generally used resistance furnaces to heat multiple grains of K-feldspar. Controlled laser-heating significantly improves our ability to quantify diffusion kinetics for several reasons. Unlike a resistance furnace, Pl–Ir envelopes produce no detectible blanks over the temperature range of interest. By minimizing the volume of heated metal, thereby minimizing blanks, detection limits decrease by up to two orders of magnitude, enabling more precise data acquisition from smaller samples. Another key aspect of this heating technique is the ability to rapidly and accurately reach the desired set-point temperature without overshooting, which is detrimental to a diffusion experiment and essentially impossible to achieve with either a resistance furnace or laser heating without pyrometry. Due to the small mass and high-thermal conductivity of the metal envelopes, samples cool rapidly (<30 s) upon cessation of heating. Therefore, uncertainties associated with thermal lag and thermal drift are virtually eliminated. The heating technique not only enables detailed diffusion analyses of individual plagioclase crystals, but is also applicable to K-feldspar, pyroxene, and other anhydrous minerals whose degassing kinetics are unrelated to devolatilization processes.

4.2. Experimental details

We first gently crushed a whole-rock sample using a mortar and pestle, and then hand picked plagioclase
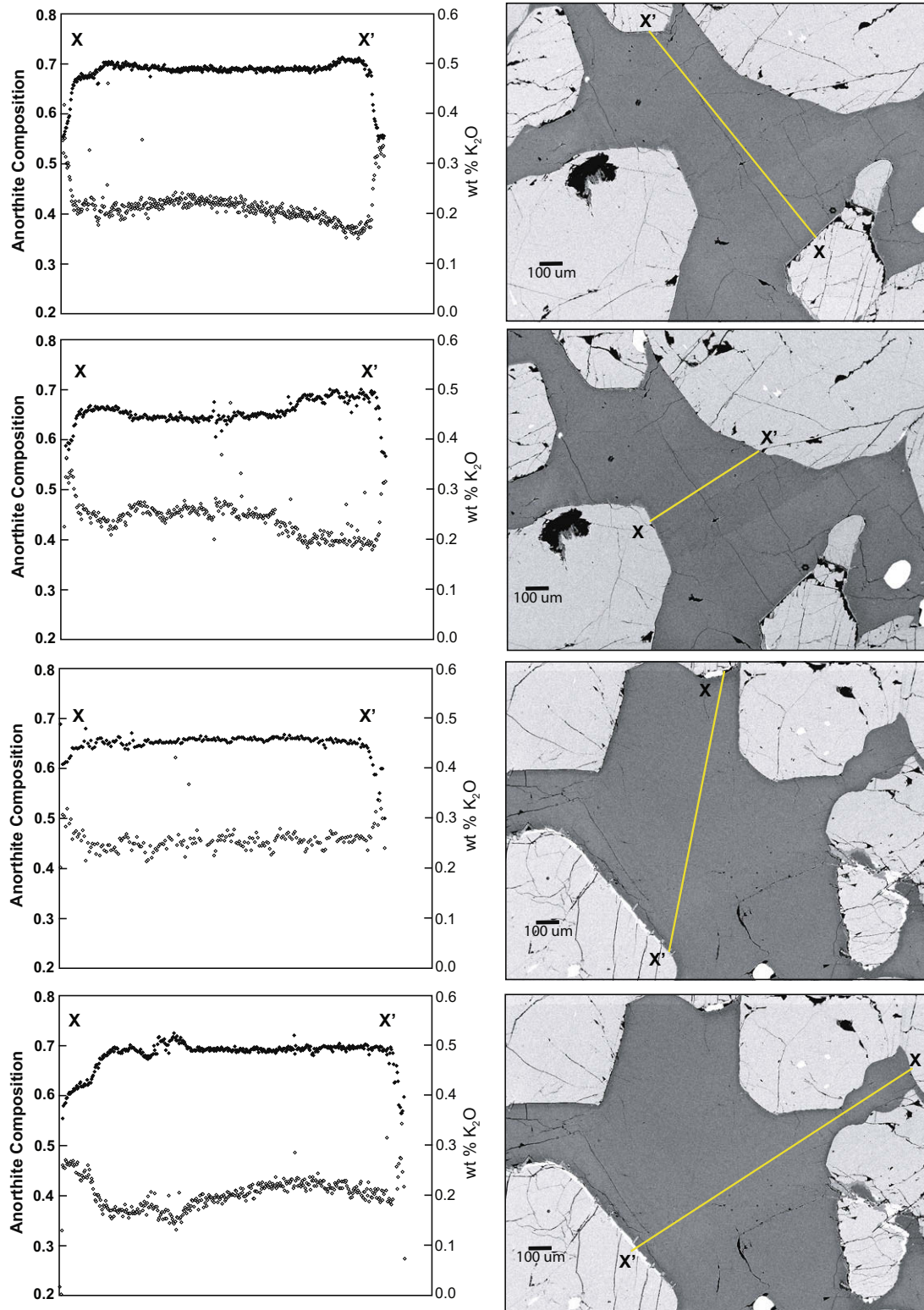
Fig. 3. Backscattered electron images of representative BV-8 plagioclase grains. Yellow lines indicate microprobe traverse paths. Chemical compositions measured every 2 μm along the paths using a 1 μm beam diameter are plotted to the left of corresponding images. Bold, filled symbols denote anorthite composition, plotted on the primary y-axis. Open symbols denote wt. K_2O, plotted on the secondary y-axis. The plagioclase crystals are bimodal, with both an An_{70} and An_{40} population. K_2O concentrations are typically 0.2 wt.%. Individual plagioclase grains are compositionally homogenous at the μm scale. Most crystals are considerably zoned, with higher K and lower Ca concentrations toward grain edges, as well as in narrow intercumulus regions, which were removed during sample preparation. (For interpretation of the references to color in this figure legend, the reader is referred to the web version of this paper.)

crystals 0.5–1.5 mm in diameter under a binocular microscope. We avoided fragments of once larger grains or heavily fractured grains; age spectra of broken fragments may not reflect the original ^{40}Ar gradient across intact grains. Selected grains preserved the dimensions inherent to the intercumulus texture we observed in hand sample and thin section. The plagioclase crystals were loaded into aluminum discs alongside Fish Canyon sanidine (FCs; 28.02 Ma) flux monitors (Renne et al., 1998). The samples and flux monitors were co-irradiated for 100 h at the Oregon State University TRIGA reactor in the Cadmium-Lined In-Core Irradiation Tube (CLICIT). Individual crystals, identified as BV-8-X, where X refers to a single grain, were then loaded into small metal packets made from high-purity, 2 mm long Pt–Ir tubes (1 mm in diameter with a .05 mm wall thickness), crimped at both ends to create an encapsulating "envelope", and placed into an ultra-high vacuum system beneath a sapphire view port.

Samples were heated with a 30 W diode laser ($\lambda = 810 \pm 10$ nm) that efficiently couples with Pl–Ir. The diode laser was focused onto the metal envelope and coaxially aligned with an optical, single-color pyrometer. The pyrometer's temperature output fed back into a PID temperature controller to drive the laser output power. This feedback loop operates at a frequency of 1 Hz. To account for emissivity variations, it was necessary to calibrate the single-color pyrometer output against a type-K thermocouple under high-vacuum. During experimental heating, the sample is held at a controlled temperature for known time duration.

Heating duration ranged from 300 to 1200 s, with longer times used at lower temperatures in order to generate measurable amounts of argon. Samples were fused at the completion of the incremental-heating analyses. The released argon was purified and analyzed using Mass Analyzer Products 215–50 mass spectrometer and measured statically on a Balzers SEV-217 electron multiplier using procedures similar to those described by Renne et al. (1998). Corrections were made for interfering nuclear reaction products (Renne et al., 2005), ^{37}Ar and ^{39}Ar decay, spectrometer discrimination, and extraction line blanks. Mass discrimination (1.0075 ± 0.0015 per atomic mass unit) based on a power law relationship (Renne et al., 2009) was determined from analysis of 32 aliquots from an automated air pipette system, interspersed with the unknowns. Apparent ages (Fig. 4, data in the Electronic Annex) were calculated using an age of 28.02 Ma for FCs and the constants of Steiger and Jäger (1977).

4.3. Regression criteria for Arrhenius plots

To quantify diffusion kinetics, we used both ^{37}Ar and ^{39}Ar data, since these isotopes have essentially zero contribution from atmospheric blank and are *a priori* expected to have a uniform spatial distribution in the irradiated crystals. Simultaneously examining both ^{37}Ar and ^{39}Ar permits directly assessing the fundamental assumption in our calculations that Ca and K, and hence ^{37}Ar and ^{39}Ar, are uniformly distributed (see below). Using the fraction of ^{37}Ar or ^{39}Ar and the duration of each step, we calculate the
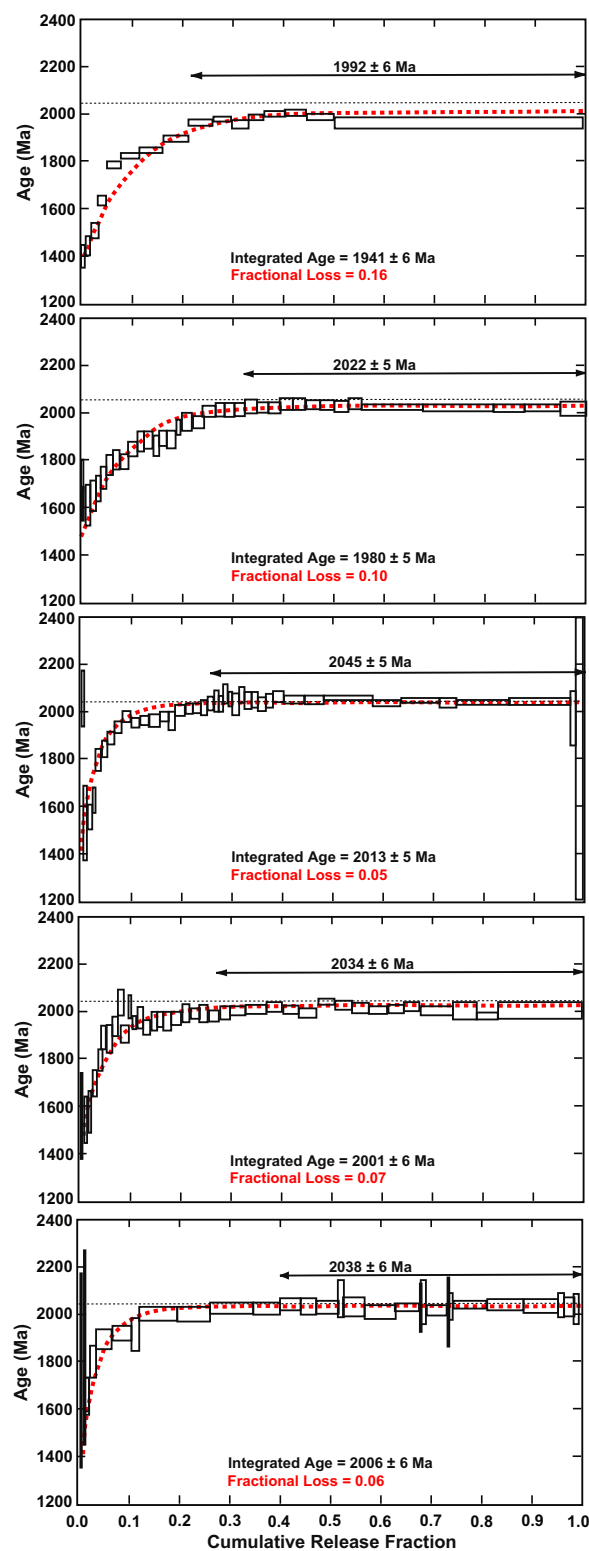

Fig. 4. Apparent age spectra for BV-8-1 to BV-8-5 (top to bottom). Model age spectra are shown as dashed red lines and were calculated assuming that BV-8 was intruded at 2045 Ma (fine dashed black line) and remained closed to argon loss after 1400 Ma, as required by the apparent ages of initial steps. Arbitrary "plateau" ages are shown above the age spectra to indicate maximum age. (For interpretation of the references to color in this figure legend, the reader is referred to the web version of this paper.)

diffusion coefficient (D) normalized to the characteristic length scale (D/a^2) using the equations of Crank (1975), assuming plane slab geometry. Plane slab was chosen as the preferred geometry as age spectra closely conform to model plane slab diffusion loss profiles for the calculated fractional gas losses (Fig. 4; see Section 5.1). Model spherical diffusion loss spectra do not reproduce the observed age spectra as well for the calculated fractional gas losses because spherical diffusion loss profiles progressively increase in age without establishing apparent plateaus, as in plane slab diffusion loss profiles. It is worth noting that plane slab geometry is commonly used in calculating Ar diffusion kinetics in K-feldspar (e.g., Lovera et al., 1989, 1991, 1997), and anisotropic cation diffusion in plagioclase has been documented in a number of studies (e.g., Cherniak, 1995; Giletti and Shanahan, 1997).

Uncertainties in calculated D/a^2 are directly related to the analytical precision of each step. We ignore any uncertainty contributed from the cumulative release fraction, as each step is dependent upon all previous steps and would produce significant error correlations if included (Lovera et al., 1991). Uncertainty on the temperature is conservatively estimated to be $\pm 5\ ^\circ C$ (1σ). We quantified temperature dependence of the diffusion coefficient from weighted linear regression models of $\ln(D_0/a^2)$ against $1/T$ using Isoplot 3.0 (Ludwig, 2003). Acceptable regressions include the maximum number of consecutive low-temperature steps preceding unambiguous departures from linear Arrhenius arrays and are required to yield statistically indistinguishable diffusion parameters for both ^{37}Ar and ^{39}Ar (at the 2σ level). On occasion, initial steps (comprising less than less than 0.05% of the gas) were excluded if they differed significantly from linear Arrhenius arrays defined by subsequent extractions.

The heating schedule that optimizes the information on the Arrhenius plot may yield a suboptimal age spectrum owing to insufficient quantities of radiogenic argon release. Specifically, cycled heating experiments reveal detailed diffusion data and test fundamental assumptions in the experiment, but ages determined during retrograde heating steps are exceedingly imprecise and of little geochronological significance as the ^{40}Ar signal to background ratio is negligibly above 1. Abundances of ^{37}Ar and ^{39}Ar obtained during retrograde heating are significantly larger than background as they are non-atmospheric isotopes. Retrograde heating steps typically amount to less than 0.5% of the total gas released and can be neglected in age spectra calculations. Uncertainties on ages are quoted at the 1σ level and include the uncertainty in the irradiation parameter J, which is typically $\sim$0.5%.

5. RESULTS

5.1. Geochronology

BV-8 age spectra are consistent with thermally activated diffusive loss from a single domain (Fig. 4). The discordant age spectra are most simply explained by either (1) partial degassing of the sample by a thermal event at $\sim$1.4 Ga such as intrusion of the Pilanesberg Complex or (2) protracted cooling of the Bushveld Complex, followed by exhumation to shallow crustal depths (<3 km) at $\sim$1.4 Ga. Ambiguity between late-stage loss and slow cooling inferred from ^{40}Ar/^{39}Ar data has been discussed at length in previous texts (e.g., McDougall and Harrison, 1999).

To obtain estimates of radiogenic argon loss we assumed that BV-8 was intruded at 2045 Ma, corresponding to the maximum plateau age computed using the standard age and decay constant of Renne et al. (1998) and Steiger and Jäger (1977), respectively. More accurate ages follow from improved calibrations (e.g., $\sim$2057 Ma when calibrated to the U–Pb consistent values of $t_{FCs} = 28.28$ Ma and $\lambda_{40K} = 5.53^{-10}a^{-1}$ (Mundil et al., 2006), or 2054 Ma using $t_{FCs} = 28.201$ Ma of Kuiper et al. (2008) and the ^{40}K decay constant of Mundil et al. (2006)), but for the present purposes the choice of age calibrations is unimportant. The youngest ages observed in the initial steps require that the plagioclase crystals remained closed to argon loss after 1400 Ma. Therefore, fractional loss (F) of each grain is easily calculated using the integrated age (A_I).

$$F = \frac{e^{\lambda*(2045-1400)\mathrm{Ma}} - e^{\lambda*(A_I-1400)\mathrm{Ma}}}{e^{\lambda*(2045-1400)\mathrm{Ma}} - 1}, \tag{1}$$

where A_I is simply the ^{40}Ar/^{39}Ar age calculated from the sum of all steps. Individual grains have lost between $5.0 \pm 0.8\%$ and $16.1 \pm 1.0\%$ of their radiogenic argon (Table 1), where the 1σ uncertainty was propagated from the uncertainty on the integrated age. Model age spectra for the calculated fractional losses are shown alongside the real age spectra in Fig. 4.

5.2. Diffusion kinetics

Single grains were subjected to one of three different types of heating schedules: monotonically increasing, monotonically increasing with duplicate isothermal steps, or cycled heating with duplicate isothermal steps. Arrhenius plots are shown alongside the heating schedules and Ca/K spectra in Figs. 5, 6 and 7 and in the Electronic Annex Figs. 2 and 3. In general, ^{37}Ar and ^{39}Ar behave somewhat differently during low-temperature extractions between 350 and $\sim$700 °C. D_0/a^2 values calculated from ^{39}Ar yield curvilinear to convex-up arrays with that are roughly 10 times higher than those from ^{37}Ar. The ^{37}Ar values produce highly linear arrays through this temperature range. The ^{39}Ar results yield lower apparent activation energies than ^{37}Ar at lower temperatures. Qualitatively similar results were also observed in plagioclase by Harrison and McDougall (1981) and Onstott et al. (1989). Upon heating to 700–800 °C, the calculated ^{39}Ar diffusivities converge with ^{37}Ar diffusivities. Initial extractions resulting in apparently high ^{39}Ar D_0/a^2 values coincide with relatively low Ca/K ratios (Figs. 5c, 6c and 7c), which we infer to result from compositional zoning (K-enrichment) near grain edges. A plot of ΔCa/K, the difference between the Ca/K plateau ratio and that of a given step, vs. ΔD_{37}:D_{39}, the difference between the diffusion coefficients of ^{37}Ar and ^{39}Ar, illustrates the relationship (Figs. 5d, 6d and 7d).

Electron microprobe traverses indicate that K_2O concentrations increase by nearly a factor of two toward the

Table 1
Summary of diffusion parameters.

Sample	Ave. Ca/K	Total Gas Age Ma ± 1σ	Frac. loss F ± 1σ	Argon isotope	Steps used	MSWD	$E_a \pm 1\sigma$ (kJ/mol)	$\ln(D_o/a^2) \pm 1\sigma$ (ln(s^{-1}))	$T_c \pm 1\sigma$ (°C)
BV-8-1	55	1941 ± 6	0.161 ± 0.010	37	1–13	0.30	158.3 ± 3.6	4.18 ± 0.39	232 ± 6
				39	6–13	1.02	144.7 ± 6.7	3.26 ± 0.68	200 ± 13
				Weighted average			**155.3 ± 3.1**	**3.95 ± 0.34**	**225 ± 6**
BV-8-2	30	1980 ± 5	0.101 ± 0.008	37	1–26	0.61	165.7 ± 3.0	5.25 ± 0.31	241 ± 5
				39	6–26	0.89	151.8 ± 4.1	3.93 ± 0.40	215 ± 8
				Weighted average			**161.2 ± 2.5**	**4.75 ± 0.25**	**233 ± 5**
BV-8-3	60	2013 ± 5	0.050 ± 0.008	37	2–19	1.06	178.9 ± 2.2	5.61 ± 0.22	276 ± 3
				39	11–17	0.28	169.5 ± 7.9	5.09 ± 0.89	254 ± 13
				Weighted average			**178.4 ± 2.1**	**5.58 ± 0.22**	**275 ± 3**
BV-8-4	65	2001 ± 6	0.068 ± 0.010	37	6–36	0.80	172.0 ± 2.9	6.46 ± 0.32	244 ± 5
				39	23–36	0.46	159.6 ± 10.0	5.20 ± 0.80	223 ± 20
				Weighted average			**170.8 ± 2.7**	**6.29 ± 0.30**	**243 ± 4**
BV-8-5	80	2006 ± 6	0.061 ± 0.009	37	1–19	0.52	180.4 ± 6.7	4.02 ± 0.95	303 ± 6
				39	9–19	0.51	158.8 ± 13.7	1.90 ± 1.80	264 ± 19
				Weighted average			**176.3 ± 6.1**	**3.60 ± 0.85**	**296 ± 6**

All ages calculated using the decay constants of Steiger and Jäger (1977) ($\lambda_{40K} = 5.543 \times 10^{-10}$ y^{-1}) and corrected for ^{37}Ar and ^{39}Ar decay, half lives of 34.95 days and 269 years, respectively.
J-value calculated relative to 28.02 ± 0.20 Ma for the Fish Canyon sanidine.
T_c calculated assuming a cooling rate of 10 °C/Ma.

marginal 1–3 radial-% of BV-8 plagioclase grains, while CaO concentrations decrease by 0–25% (Fig. 3). High ^{39}Ar$_K$ concentration at grain margins results in (1) both inward and outward diffusion toward areas of lower concentration, and (2) apparently enhanced diffusion coefficients

for all steps extracted prior to homogenization of the enrichment as diffusion coefficients are calculated assuming a uniform concentration distribution. Conversely, lower ^{37}Ar$_{Ca}$ concentration at grain margins does not yield significantly diminished diffusion coefficients for two reasons.
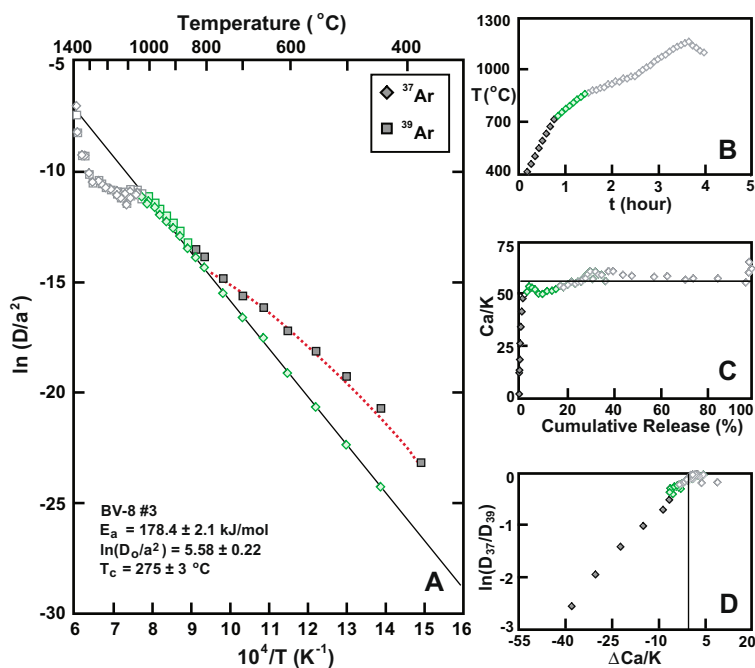

Fig. 5. (A) Arrhenius plot for BV-8-3 calculated for plane slab geometry shown alongside (B) the laboratory heating schedule, (C) the Ca/K spectra, and (D) the $\ln(D_{37}/D_{39})$ plot. Green symbols indicate steps included in diffusion parameter calculations. Weighted average diffusion parameters obtained from ^{37}Ar and ^{39}Ar data are reported in the inset. The dashed red line is a model calculated assuming a factor of two higher K concentration in the outer 2 radial-% of the grain. Uncertainties in calculated D/a^2 values are generally smaller than the symbols, but are not shown. (For interpretation of the references to color in this figure legend, the reader is referred to the web version of this paper.)
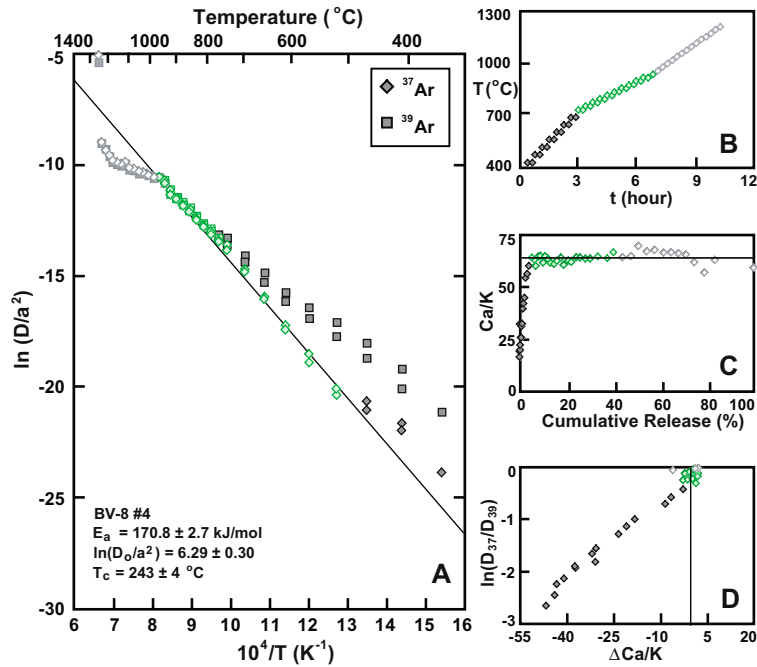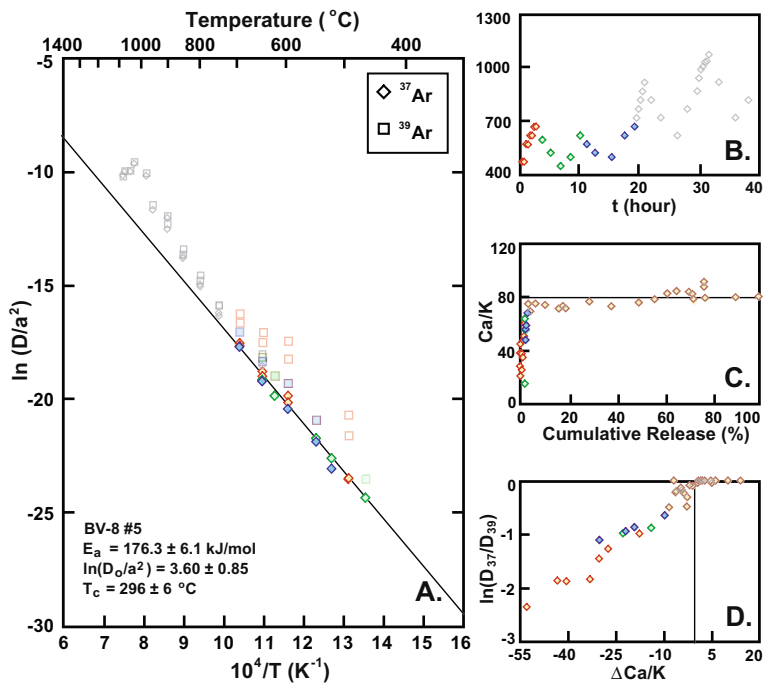
Fig. 6. (A) Arrhenius plot for BV-8-4 calculated for plane slab geometry shown alongside (B) the laboratory heating schedule, (C) the Ca/K spectra, and (D) the $\ln(D_{37}/D_{39})$ plot. Green symbols indicate steps included in diffusion parameter calculations. Weighted average diffusion parameters obtained from ^{37}Ar and ^{39}Ar data are reported in the inset. Uncertainties in calculated D/a^2 values are generally smaller than the symbols, but are not shown.

Fig. 7. (A) Arrhenius plot for BV-8-5 calculated for plane slab geometry shown alongside (B) the laboratory heating schedule, (C) the Ca/K spectra, and (D) the $\ln(D_{37}/D_{39})$ plot. Green symbols indicate steps included in diffusion parameter calculations. Weighted average diffusion parameters obtained from ^{37}Ar and ^{39}Ar data are reported in the inset. Uncertainties in calculated D/a^2 values are generally smaller than the symbols, but are not shown.

First, as diffusion progresses only out of the grain, the lower concentration at the grain margin is quickly homogenized by the higher interior concentration. Second, the relative change in ^{37}Ar$_{Ca}$ concentration (0–25%) is far less

significant than the relative change in $^{39}Ar_K$ concentration (up to 100%). Allowing for zoning within these limits, we simulated grain-scale diffusion from BV-8-3 using the diffusion parameters shown in Fig. 5. Modeled D_0/a^2 values assuming a twofold increase in K concentration in the outer 2 radial-% of the grain are shown as the dashed red line in Fig. 5a. Clearly K-enrichment near grain edges can explain the Arrhenius behavior of BV-8-3, implying that grain-scale diffusion dominates argon transport in this relatively simple plagioclase. An alternative explanation for differential low-T Arrhenius behavior was given by Harrison and McDougall (1981), in which ^{37}Ar and ^{39}Ar diffuse from different exsolution lamellae of different length scales and/or diffusion kinetics. However, as BV-8 plagioclase do not have μm scale anti-perthite lamellae, and reactor-induced recoil would likely obscure any nanometer-scale compositional variations, this rationale is not applicable. Furthermore, Parsons et al. (1999) concluded that coherent perthitic intergrowths do not provide significant fast pathways for Ar loss.

Between ~700 and 900–1000 °C the calculated diffusivities of ^{37}Ar and ^{39}Ar are indistinguishable and share the same apparent kinetics. Extractions at these temperatures are characterized by uniform Ca/K ratios and, together with the low-temperature data for ^{37}Ar, yield activation energies of 155–178 kJ/mol and $\ln(D_0/a^2)$ values between 3.5 and 6.5 (Fig. 8, Table 1). Repeated isothermal steps in this temperature range with significant release fractions do not depart from linear arrays on Arrhenius plots. This observation strongly indicates that single-domain diffusion dominates argon transport in this plagioclase. The observed diffusion parameters correspond to closure temperatures of 225–300 °C (for a 10 °C/Ma cooling rate; Fig. 8). D_0/a^2 values measured above 900–1000 °C are lower than expected from linearly extrapolating the Arrhenius relationship described in the preceding paragraph. Correlations between deviations from linearity and both temperature and cumulative fraction of gas released are well illustrated by plotting the differ-
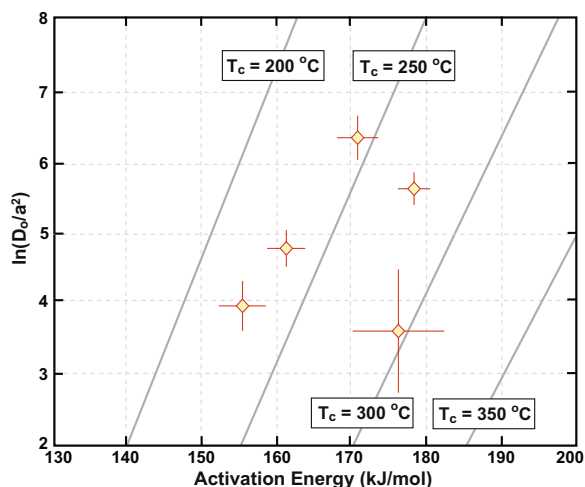
ence between the natural logarithm of a given D_0/a^2 value and that expected from the low-temperature Arrhenius relationship against these two parameters. This plot was developed by Lovera et al. (1989), wherein deviations from linearity were explicitly attributed to diffusion from multiple domains of increasing size (and constant D_o). Thus they divide $\log(D/a^2)_{calculated} - \log(D/a^2)_{Arrhenius}$ by 2, yielding $\log(r/r_o)$. In this paper we do not stipulate that departures from linearity represent a change in diffusion radius, but to avoid confusion we will maintain the nomenclature of Lovera et al. (1989), with the minor exception of plotting our deviations on the more sensitive natural log scale $(\ln(r/r_o)$; Fig. 9). Fig. 9 illustrates that BV-8-1, BV-8-2, BV-8-3, and BV-8-4 begin to significantly depart from linearity between 900 and 1000 °C, depending on the heating schedule. Departures do not correlate with the cumulative fraction of gas released, which varies between 0.18 and
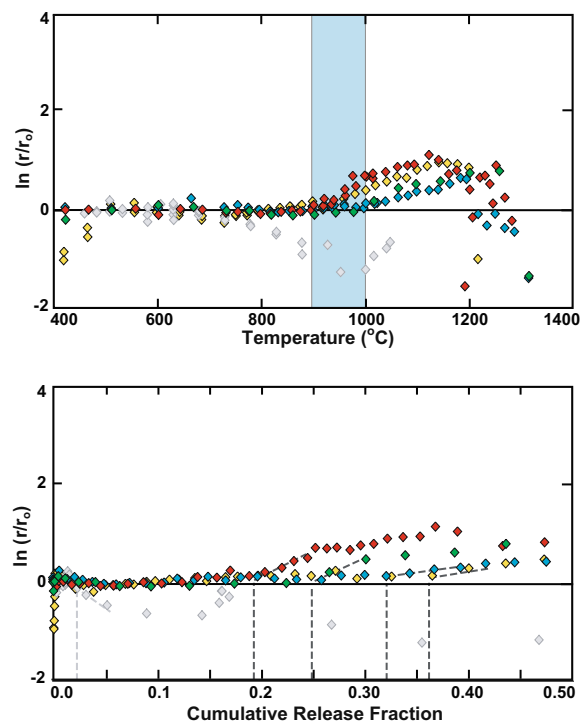

Fig. 9. Plots of $\ln(r/r_0)$ vs. temperature (above) and cumulative fraction of gas released (below). Ln(r/r_0) is the difference between the natural log of a given diffusion coefficient (D_0/a^2) and that expected from the Arrhenius relationship (using the E_a and $\ln(D_0/a^2)$ values listed in Table 1). If no difference exists, the step will plot at $\ln(r/r_0) = 0$. BV-8-1 (blue), BV-8-2 (green), BV-8-3 (red), and BV-8-4 (yellow) begin to exhibit significant departures from linear Arrhenius arrays between 900 and 1000 °C (indicated by the light blue zone), depending on the heating schedule. Departures do not appear to correlate with cumulative fraction of gas (^{37}Ar) released, which varies between 0.19 and 0.47 at the onset of deviations from linear arrays on Arrhenius plots. For BV-8-5 (grey), extensive heating (>20 h) between 400 and 700 °C (Fig. 7B) appears to have caused the sample to depart from the Arrhenius array at a lower temperature. (For interpretation of the references to color in this figure legend, the reader is referred to the web version of this paper.)

Fig. 8. Kinetic parameters for Ar diffusion in BV-8 plagioclase. Lines correspond to closure temperatures (for 10 °C/Ma) between 200 and 350 °C.

0.37 at the onset of deviations from linear arrays on Arrhenius plots (Fig. 9). Therefore, "kinks" on Arrhenius plots appear strongly related to temperature, presumably related to either (1) the onset of structural decomposition that hinders Ar diffusion (i.e., incongruent melting), (2) the development of internal microfractures in response to thermal stress (development of Ar "sinks"), or (3) annealing of intrinsic defect networks that govern diffusion (reducing D_o).

One cycled heating experiment (BV-8-5) revealed somewhat anomalous behavior (Fig. 7). While cycled heating below 800 °C did not produce significant departures from the initial low-T linear Arrhenius array, the extensive low-temperature heating (>20 h) appears to have resulted in departure from the Arrhenius array at a lower temperature than that observed in the samples which were not cycled (800 °C vs. 900–1000 °C). Between 800–1000 °C data from the cycled heating experiment trend toward higher $\ln(D_0/a^2)$ values (Fig. 7). Above 1000 °C a kink toward lower $\ln(D_0/a^2)$ values is observed (Fig. 7). The microstructural transitions that may attend these observations are not presently understood. We hope that future TEM analyses provide insights.

6. DISCUSSION

Since E_a often correlates with $\ln(D_0/a^2)$ and both are required to quantify diffusion, it is useful to characterize the diffusion kinetics of a sample by its "closure temperature" at a given cooling rate (Dodson, 1973). The closure temperature (T_c) incorporates both E_a and $\ln(D_0/a^2)$. In Fig. 10, relative grain volumes are plotted against T_c (calculated assuming a 10 °C /Ma cooling rate). Relative volumes were

determined by dividing the total ^{39}Ar of each sample by that of BV-8-5, which has the highest total ^{39}Ar. Because K_2O concentration in all grains is approximately equal (Fig. 3), the total ^{39}Ar abundance in each sample is a relative proxy for crystal volume. If the activation energy of BV-8-2 characterizes Ar diffusion in all five grains and differences in $\ln(D_0/a^2)$ values are only due to grain size variations, we expect data to plot on the dashed line (Fig. 10). Thus Fig. 10 illustrates that while some of the observed spread in T_c may result from differences in grain size, grain size cannot alone explain the observed variations. The data are also inconsistent with diffusivity varying as a function of ionic porosity, as suggested by some previous studies (e.g., Fortier and Giletti, 1989; Dahl, 1996), because ionic porosity of the analyzed grains are not expected to be different from one another.

The diffusion kinetics of individual plagioclase crystals appear to be intrinsically different, as was found to be the case with K-feldspar (e.g., Harrison et al., 1991; Lovera et al., 1997). Inherent variations in Ar diffusivity in a crystalline solid may originate from differences in the quantity, orientation, and interaction of structural and chemical defects that collectively enhance lattice diffusion (e.g., impurities, microfractures, and vacancies), as well as subtle variations in shape and chemical zoning. While structural imperfections could arise during sample preparation, we implicitly assume that the observed diffusion kinetics apply over geologic timescales and conditions.

If the observed diffusion parameters accurately quantify Ar diffusion kinetics in each plagioclase crystal, they should correlate with the apparent Ar retention exhibited in the age spectra (i.e., the most retentive grains should have the least discordant age spectra). A plot of fractional loss (F) vs. T_c indicates that F is inversely related with argon retentivity (Fig. 11). This internal consistency strongly suggests that (a) the observed diffusion kinetics are accurate and geologically meaningful, (b) significant differences exist between the five aliquots, and (c) the combined dataset should
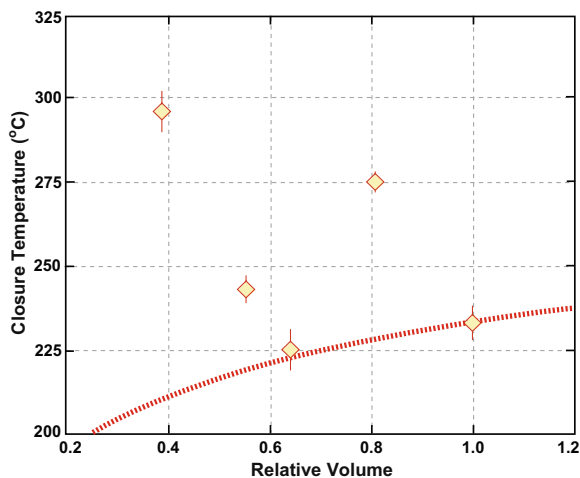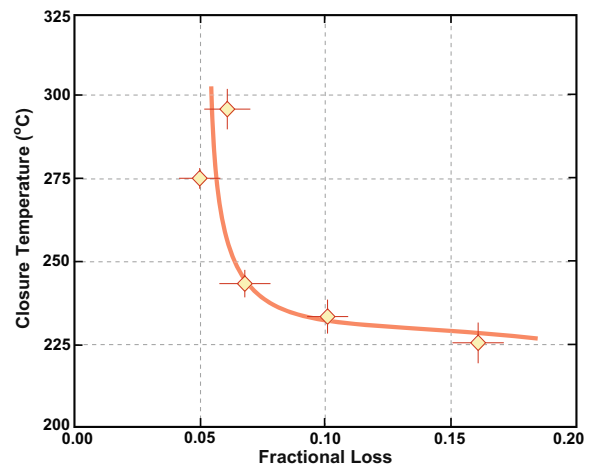

Fig. 10. Plot of relative crystal volume vs. closure temperature (calculated assuming a 10 °C /Ma cooling rate). If argon diffusion in plagioclase were characterized by specific values of E_a and D_0 (those of BV-8-2 are arbitrarily used here as it is the largest grain), closure temperature variations due to grain size differences are expected to plot on the dashed red curve. Thus, while grain size may account for some of the observed variance in closure temperature, it appears individual plagioclase crystals have intrinsically different diffusion kinetics.

Fig. 11. Plot of fractional loss (see text for calculation) vs. closure temperature (calculated assuming a 10 °C/Ma cooling rate). Fractional loss (F) is inversely correlated with closure temperature (i.e., the most retentive grains have the least disturbed age spectra).

provide a detailed constraint on the thermal history of the Bushveld Complex. As noted above, BV-8 age spectra are most simply explained either by (1) partial degassing of the Bushveld Complex by a younger intrusion, or (2) protracted cooling at elevated crustal temperatures. We quantitatively test these hypotheses in the following sections.

6.1. Reheating

Assuming plane slab geometry, the fractional Ar loss (F; see Section 5.1 and Table 1) is related to the dimensionless parameter Dt/a^2 by the following equation:

$$F \cong \frac{2}{\sqrt{\pi}}\left(\frac{Dt}{a^2}\right)^{\frac{1}{2}} \quad \text{for } F < 0.6 \qquad (2)$$

According to the Arrhenius relationship,

$$\frac{D}{a^2} = \frac{D_0}{a^2}e^{\left(\frac{-E_a}{RT}\right)} \qquad (3)$$

Substituting Eq. (3) into Eq. (2) yields

$$F \cong \frac{2}{\sqrt{\pi}}\left(t \times \frac{D_0}{a^2}e^{\left(\frac{-E_a}{RT}\right)}\right)^{\frac{1}{2}} \qquad (4)$$

Therefore, after substituting D_o/a^2 and E_a into Eq. (4), we are left with an expression for F as a function of T and t.

For each BV-8 grain, families of $T - t$ solutions that would predict F were calculated and the results are shown in Fig. 12. Upper and lower limits correspond to $T - t$ solutions calculated with E_a and $D_o/a^2 + 2\sigma$ and E_a and $D_o/a^2 - 2\sigma$, respectively. If the fractional losses observed in each BV-8 grain resulted from an instantaneous heating event, the $T - t$ fields in Fig. 12 would overlap and the mutual intersection would designate reheating solutions common to all BV-8 grains. We find no $T - t$ solutions common to all five grains, and only three grains have inter-

secting $T - t$ fields. As these grains are from the same hand sample and therefore a priori experienced the same thermal history, the discordant age spectra cannot result from a single episodic reheating event, but require a more complex cooling history or multi-stage reheating.

6.2. Slow cooling

BV-8 age spectra can also be predicted by cooling at elevated crustal temperatures if sufficiently high to permit significant argon diffusion over an extended duration. We simulated over 5000 possible thermal histories for the cooling of a half-space, given by:

$$T(z, r, t) = T_0 + (T_S - T_0)erfc\left(\frac{z}{2\sqrt{\kappa t}}\right)$$
$$+ \left[z\left(\frac{dT}{dz}\right) - rt\right] \qquad (5)$$

where T_0 is the initial temperature, which must be sufficiently high such that Ar retention in plagioclase is negligible (500 °C), T_S is surface temperature (25 °C), κ is the thermal diffusivity typical for mafic rocks (1 mm²/s), t is time, and z is the depth of intrusion. The terms in the brackets characterize the ambient temperature at the depth of intrusion, where dT/dz is the geothermal gradient (25 °C/km) and r is the rate at which the ambient temperature diminishes (°C/Ma). The term r is intended to account for both relaxation of the geothermal gradient following heightened magmatic activity as well as cooling due to erosion and uplift. For each thermal history, model age spectra were generated for all five BV-8 grains. These model age spectra were compared to the observed age spectra, and the thermal history that that yielded the lowest overall mean squared weighted deviation (MSWD) for all five grains is shown in Fig. 13. Cooling histories that resulted in less than a twofold increase in deviation are shown alongside the best-fit solution as an indicator of the goodness of fit.

Assuming a geothermal gradient of 25 °C/km and a surface temperature of 25 °C, the results of the model indicate that the Bushveld Complex was intruded at a depth of 5.1 km, cooled rapidly from magmatic temperatures to <300 °C within 3 Ma, and gradually passed through crustal temperatures of 150–200 °C over 600 Ma ($r = 0.02$ °C/Ma). Our predicted intrusion depth of 5.1 km is consistent with that inferred from stratigraphy (Fig. 2). The best-fit solution has a moderately large MSWD of 4.95, which largely reflects the inability of this overly simple model to fully capture changes in cooling and uplift rate, as the samples are constrained to cool linearly through time. A more detailed thermal model accommodating complex cooling paths and featuring samples from several localities throughout the Bushveld Complex will be the subject of a subsequent paper.
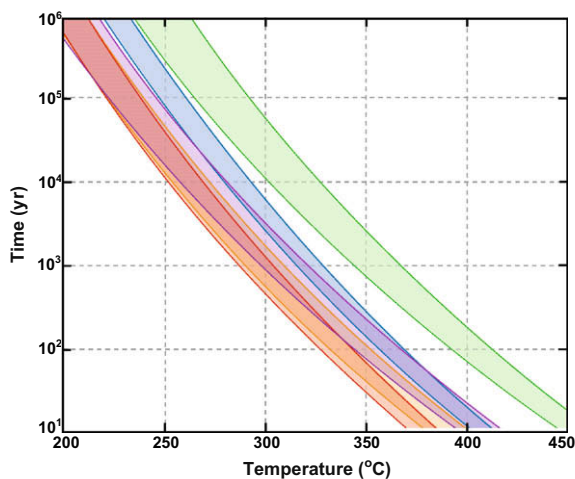

Fig. 12. $T - t$ solutions to F, the fractional loss, for BV-8-1 (blue), BV-8-2 (orange), BV-8-3 (purple), BV-8-4 (red), and BV-8-5 (green), calculated for diffusive loss at a constant temperature (T) for duration time (t) (see text for calculation). Upper and lower limits correspond to $T - t$ solutions calculated with E_a and $D_o/a^2 + 2\sigma$ and E_a and $D_o/a^2 - 2\sigma$, respectively.

7. CONCLUSIONS

Five detailed diffusion experiments on single crystals of plagioclase from a gabbro in the Bushveld Complex, South Africa, yield activation energies of 155–178 kJ/mol and
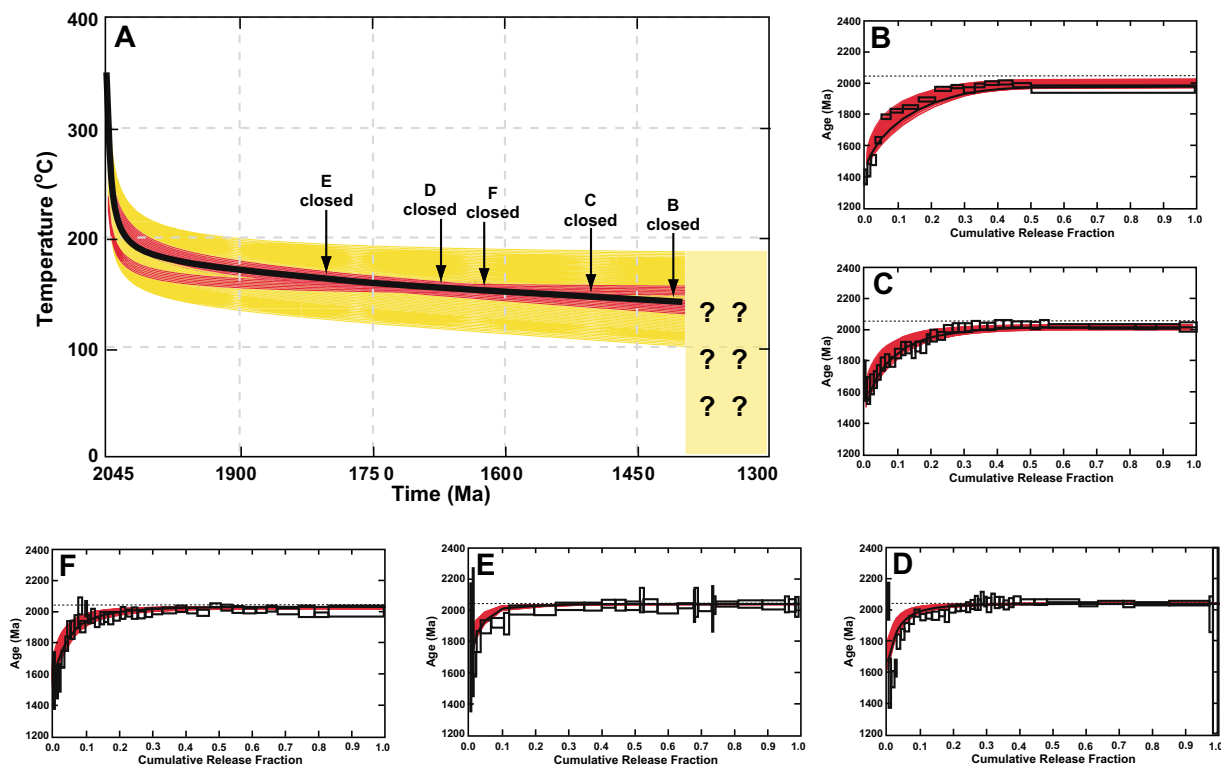
Fig. 13. (A) The most probable thermal history (black) fit to all five BV-8 age spectra (see text for calculation). Red lines correspond to thermal histories that resulted in less than a twofold increase in deviation and the yellow field corresponds to all cooling curves modeled in which the depth of intrusion is between 3 and 6 km. Model age spectra are shown alongside the observed age spectra in the surrounding panels (B. BV-8-1; C. BV-8-2; D. BV-8-3; E. BV-8-5; F. BV-8-4). The time at which each sample becomes effectively 100% closed with respect to Ar diffusion (the complete retention age) is noted on the cooling curve. At times more recent than ~1425 Ma the thermal history is constrained to remain below ~150 °C (the temperature at the time of the youngest complete retention age). (For interpretation of the references to color in this figure legend, the reader is referred to the web version of this paper.)

$\ln(D_0/a^2)$ values between 3.5 and 6.5. These diffusion parameters correspond to closure temperatures of 225–300 °C for a 10 °C/Ma cooling rate. The observed diffusion kinetics predict the differences in discordance observed in the age spectra. BV-8 age spectra generally conform to single-domain diffusive loss profiles, suggesting that grain-scale diffusion dominates argon transport in this homogenous plagioclase. The causes of observed differences in diffusion kinetics between the plagioclase grains are not presently understood, but the differences appear to be inherent to each grain. It appears that natural variations in plagioclase Ar diffusion kinetics preclude a generically applicable set of diffusion parameters unless large uncertainties are ascribed to them. Pending identification of the specific variables governing Ar diffusivity in plagioclase, assigning closure temperatures more accurate than ±100 °C requires that Ar diffusion kinetics be quantified for each sample of interest.

In the Bushveld Complex, our five single-grain analyses enable us to distinguish episodic reheating from slow cooling. No single pulse-heating event is capable of producing the fractional losses observed in all five age spectra, given the diffusion parameters determined from ^{37}Ar and ^{39}Ar release in the laboratory. Our results indicate that following intrusion the gabbro represented by sample BV-8 cooled rapidly and monotonically from magmatic temperature to

<300 °C, followed by protracted cooling to ambient crustal temperatures of 150–200 °C over ~600 Ma.

APPENDIX A. SUPPLEMENTARY DATA

Supplementary data associated with this article can be found, in the online version, at doi:10.1016/j.gca.2009.07.017.

REFERENCES

Berger G. W. and York D. (1981) Geothermometry from ^{40}Ar/^{39}Ar dating experiments. *Geochim. Cosmochim. Acta* **45**, 795–811.

Boven A., Pasteels P., Kelley S. P., Punzalan L., Bingen B. and Demaiffe D. (2001) ^{40}Ar/^{39}Ar study of plagioclases from the Rogaland anorthosite complex (SW Norway): an attempt to understand argon ages in plutonic plagioclase. *Chem. Geol.* **176**, 105–135.

Buick I. S., Maas R. and Gibson R. (2001) Precise U–Pb titanite age constraints on the emplacement of the Bushveld Complex, South Africa. *J. Geol. Soc. Lond.* **158**, 3–6.

Campbell I. H., Griffiths R. W. and Hill R. I. (1989) Melting in an Archean mantle plume: heads it's basalt, tails it's komatiite. *Nature* **339**, 697–699.

Cawthorn R. G. and Walraven F. (1998) Emplacement and crystallization time for the Bushveld Complex. *J. Petrol.* **39**, 1669–1687.

Cherniak D. J. (1995) Diffusion of lead in plagioclase and K-feldspar: an investigation using Rutherford Backscattering and Resonant Nuclear Reaction Analysis. *Contrib. Mineral. Petrol.* **120**, 358–371.

Crank J. (1975) *The Mathematics of Diffusion*, secod ed. Clarendon Press, Oxford.

Dahl P. S. (1996) The crystal-chemical basis for Ar retention in micas: inferences from interlayer partitioning and implications for geochronology. *Contrib. Mineral. Petrol.* **123**, 22–39.

Dodson M. H. (1973) Closure temperature in cooling geochronological and petrological systems. *Contrib. Mineral. Petrol.* **40**, 259–274.

Eales H. V. and Reynolds I. M. (1986) Cryptic variation within chromites of the Upper Critical Zone, northwestern Bushveld Complex. *Econ. Geol.* **81**, 1056–1066.

Fechtig H., Gentner W. and Zähringer J. (1960) Argon Bestimmungen an Kaliumminerlien-VII. Diffusionsverluste von Argon in Mineralien und ihre Auswirkung auf die Kalium–Argon–Altersbestimmung. *Geochim. Cosmochim. Acta* **19**, 70–79.

Fechtig H. and Kalbitzer S. (1966) The diffusion of argon in potassium bearing solids. In *Potassium–Argon Dating* (eds. O. A. Schaeffer and J. Zahringer). Springer, pp. 68–106.

Fortier S. M. and Giletti B. J. (1989) An empirical model for predicting diffusion coefficients in silicate minerals. *Science* **245**, 1481–1485.

Garrick-Bethell I., Weiss B. P., Shuster D. and Buz J. (2009) Early lunar magnetism. *Science* **323**, 356–359.

Giletti B. J. and Shanahan T. M. (1997) Alkali diffusion in plagioclase feldspar. *Chem. Geol.* **139**, 3–20.

Harrison T. M. and McDougall I. (1981) Excess ^{40}Ar in metamorphic rocks from broken hill, New-South-Wales – implications for ^{40}Ar/^{39}Ar age spectra and the thermal history of the region. *Earth Planet. Sci. Lett.* **55**, 123–149.

Harrison T. M., Lovera O. M. and Heizler M. T. (1991) ^{40}Ar/^{39}Ar results for alkali feldspars containing diffusion domains with differing activation energy. *Geochim. Cosmochim. Acta* **55**, 1435–1448.

Hess P. C. and Parmentier E. M. (1995) A model for the thermal and chemical evolution of the Moon's interior: implications for the onset of mare volcanism. *Earth Planet. Sci. Lett.* **134**, 501–514.

Jourdan F. and Renne P. R. (2007) Age calibration of the Fish Canyon sanidine ^{40}Ar/^{39}Ar dating standard using primary K–Ar standards. *Geochim. Cosmochim. Acta* **71**, 387–402.

Kuiper K. F., Deino A., Hilgen F. J., Krijgsman W., Renne P. R. and Wijbrans J. R. (2008) Synchronizing rock clocks of Earth history. *Science* **320**, 500–504.

Lovera O. M., Richter F. M. and Harrison T. M. (1989) The ^{40}Ar/^{39}Ar thermochronometry for slowly cooled samples having a distribution of diffusion domain sizes. *J. Geophys. Res.* **94**, 17917–17935.

Lovera O. M., Richter F. M. and Harrison T. M. (1991) Diffusion domains determined by ^{39}Ar release during step heating. *J. Geophys. Res.* **96**, 2057–2069.

Lovera O. M., Grove M., Harrison T. M. and Mahoni K. I. (1997) Systematic analysis of K-feldspar ^{40}Ar/^{39}Ar step heating results: I. Significance of activation energy determinations. *Geochim. Cosmochim. Acta* **61**, 3171–3192.

Ludwig, K.R. (2003). Using Isoplot/Ex, Version 2.01: A geochronological toolkit for Microsoft Excel. Berkeley Geochronology Center Special Publication, Berkeley Geochronology Center, Berkeley, CA. 1a, 47 pp.

McDougall I. and Harrison T. M. (1999) *Geochronology and Thermochronology by the ^{40}Ar/^{39}Ar Method*. Oxford University Press.

Meyer W. V. and Neldel H. (1937) Uber die Beziehungen zwischen der Energiekonstanten e und der Mengenkonstanten (Y der Leitwerts-Temperaturformel bei oxydischen Halbleitern. *Z. Technol. Phys.* **18**, 588–593.

Mundil R., Renne P. R., Min K. K. and Ludwig K. R. (2006) Resolvable miscalibration of the ^{40}Ar/^{39}Ar geochronometer. *Eos Transactions AGU* **87**, 52.

Nomade S., Renne P. R. and Merkle R. K. W. (2004) ^{40}Ar/^{39}Ar age constraints on ore deposition and cooling of the Bushveld Complex, South Africa. *J. Geol. Soc. Lond.* **161**, 411–420.

Onstott T. C., Hall C. M. and York D. (1989) ^{40}Ar/^{39}Ar Thermochronometry of the imataca complex, Venezuela. *Precambrian Research* **42**, 255–291.

Parsons I., Brown W. L. and Smith J. V. (1999) ^{40}Ar/^{39}Ar thermochronology using alkali feldspars: real thermal history or mathematical mirage of microtexture? *Contrib. Mineral. Petrol.* **136**, 92–110.

Renne P. R., Onstott T. C., D'Agrella M. S., Pacca I. G. and Teixeira W. (1990) ^{40}Ar/^{39}Ar dating of 1.0–1.1 Ga magnetizations from the são francisco and kalahari cratons: tectonic implications for Pan-African and Brasiliano mobile belts. *Earth Planet. Sci. Lett.* **101**, 349–366.

Renne P. R., Deckart K., Ernesto M., Féraud G. and Piccirillo E. M. (1996) Age of the Ponta Grossa Dike Swarm (Brazil) and implications for paraná flood volcanic province. *Earth Planet. Sci. Lett.* **144**, 199–212.

Renne P. R., Swisher C. C., Deino A. L., Karner D. B., Owens T. L. and DePaolo D. J. (1998) Intercalibration of standards, absolute ages and uncertainties in ^{40}Ar/^{39}Ar dating. *Chem. Geol.* **145**, 117–152.

Renne P. R., Knight K. B., Nomade S., Leung K.-N. and Lou T.-P. (2005) Application of deuteron-deuteron (D-D) fusion neutrons to ^{40}Ar/^{39}Ar geochronology. *Applied Radiation and Isotopes* **62**, 25–32.

Renne P. R., Cassata W. S. and Morgan L. (2009) The isotopic composition of atmospheric argon and ^{40}Ar/^{39}Ar geochronology: Time for a change? *Quaternary Geochronology* **4**, 288–298.

Scoates J. S. and Friedman R. M. (2008) Precise age of the platiniferous Merensky Reef, Bushveld Complex, South Africa, by the U-Pb zircon chemical abrasion ID-TIMS technique. *Economic Geology* **103**, 465–471.

Steiger R. H. and Jäger E. (1977) Subcommission on geochronology: convention on the use of decay constants in geo- and cosmo-chronology. *Earth and Planetary Science Letters* **5**, 320–324.

Associate editor: Peter W. Reiners